VOL. 7, NO. 3, MARCH 2012 ISSN 1819-6608
ARPN Journal of Engineering and Applied Sciences


www.arpnjournals.com

TRANSIENT-RATE ANALYSIS FOR LONG HOMOGENEOUS AND NATURALLY FRACTURED RESERVOIR BY THE *TDS* TECHNIQUE

Freddy Humberto Escobar[1], Margarita Maria Rojas[2] and Luis Fernando Bonilla[1]
[1]Universidad Surcolombiana, Av. Pastrana - Cra. 1, Neiva, Huila, Colombia
[2]Global Petroleum Systems, Bogota, Colombia
E-Mail: fescobar@usco.edu.co

ABSTRACT

Normally, production data are analyzed by decline-curve fitting. However, analogous to pressure-transient analysis, the reciprocal flow rate and its derivative may be analyzed and interpreted for reservoir characterization purposes. In some cases, formation linear flow regime may be seen once the radial flow regime vanished. This flow regime is very important and can be presented in fractured well, horizontal wells and long reservoirs. Either pressure-transient analysis or rate-transient analysis may be affected by linear flow regime. For the case of production rate at constant well-flowing pressure, most of the analysis is conducted by decline-curve analysis and little attention has been given to rate-transient analysis. This paper presents the governing equations used for rate-transient analysis in elongated systems using characteristic points and "fingerprints" found on the log-log plot of reciprocal rate and reciprocal rate derivative, so analytical expressions were developed to determine reservoir parameters, following the philosophy of the *TDS* Technique. It allows for the estimation of reservoir permeability, reservoir width and geometrical skin factors. If the test is long enough, reservoir drainage area, well position inside the reservoir and/or reservoir length can also be determined. The methodology was successfully verified by its application to synthetic cases.

Keywords: reservoir, transient rate, linear flow, parabolic flow, well-flowing pressure, reciprocal rate derivative, *TDS* technique.

RESUMEN

Normalmente, los datos de producción se analizan por medio de ajuste de curvas de declinación. Sin embargo, análogo al análisis de pruebas de presión, el recíproco del caudal y su derivada podrán analizarse e interpretarse para propósitos de caracterización del yacimiento. En algunos casos, el régimen de flujo lineal dentro de la formación podría ser visto una vez que desaparece el flujo radial. Este régimen de flujo se presenta en pozos fracturados, pozos horizontales y yacimientos alargados. Ya sea el análisis transitorio de la presión o el análisis de datos de caudal podrán estar afectados por el régimen de flujo lineal. En el caso de producción a presión de fondo constante, la mayoría del análisis se conduce mediante curvas de declinación y muy poca atención ha recibido el análisis transitorio de la tasa de flujo. En este artículo se presentan las ecuaciones gobernantes usadas en análisis transitorio del caudal para sistemas alargados usando puntos característicos y "huellas digitales" hallados en el gráfico logarítmico del recíproco del caudal y su derivada de modo que se desarrollaron expresiones analíticas para determinar los parámetros del yacimiento siguiendo la filosofía del la técnica *TDS*. Esta permite determinar la permeabilidad, el ancho del yacimiento y los daños geométricos. Si la prueba es lo suficientemente larga se pueden estimar el área de drenaje, posición del pozo dentro del yacimiento y/o la longitud del yacimiento. La metodología se verificó satisfactoriamente mediante su aplicación a ejemplos simulados.

PALABRAS CLAVES

Flujo lineal, flujo parabólico, ancho del yacimiento, presión de fondo fluyente, derivada del recíproco del caudal.

1. INTRODUCTION

Formation linear flow in vertical wells can be due to geological events (meandering), hydraulic fractures, horizontal wells, faulting or sand lens. Nutakki and Mattar (1982) presented an investigation for infinite channel reservoirs using a vertical fracture approach with a pseudo skin factor. Their governing pressure equation possesses a wrong constant but they provided the first mathematical insights to work on long and narrow reservoir systems and provided a conventional straight-line methodology for well test interpretation. Raghavan and Chu (1996) introduced a method to estimate average pressure when radial flow conditions are nonexistent for the cases of linear and bilinear flow regimes which may be applicable to channel reservoirs. Massonat *et al*., (1993) presented flow simulations in geologically complex channelized reservoirs. Their well test analysis was performed by non-linear regression analysis and no interpretation technique was presented. Wong *et al*., (1986) introduced new type curves to interpret pressure transient analysis for rectangular reservoirs. They solved some field examples using type-curve matching and conventional techniques. Their type curves allowed easy recognition of the late-time behavior for all possible well positions in the mentioned reservoir systems.

Recently, Escobar *et al*. (2007) introduced the application of the *TDS* technique for characterization of long and homogeneous reservoirs, presenting new

equations for estimation of reservoir area, reservoir width and geometrical skin factors. Escobar *et al*. (2005) introduced a new flow regime exhibiting a negative half slope on the pressure derivative curve once dual-linear flow has ended. Escobar and Montealegre (2006) studied the impact of the geometric skin factors on elongated systems. Characterization of pressure tests in elongated systems using the conventional method was also presented by Escobar and Montealegre (2007). Escobar (2008) presented a summary of the advances in characterization of long and homogenous reservoirs using pressure-transient analysis. El-Banbi and Wattenbarger (1996) were the first in applying rate-transient analysis to elongated systems. An example of this behavior can be seen in the log-log plot of the reciprocal rate versus time for a Mexican well shown in Figure-1. Escobar *et al*. (2010) presented a detailed study on the interpretation of reciprocal rate vs. time data by the straight-line conventional analysis method. They presented the governing equations for heterogeneous and naturally fractured reservoir. Actually, this study is a continuation of it.

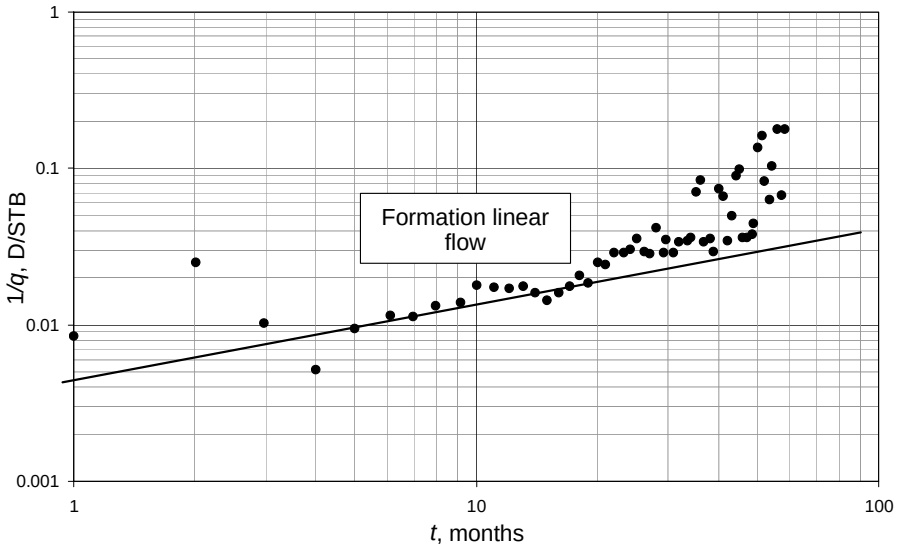

Figure-1. Evidence of formation linear flow in a constant-pressure test found in a Mexican well.

2. FORMULATION

For the mathematical development consider the following dimensionless parameters:

$$t_D = \frac{0.0002637kt}{\phi\mu c_t r_w^2} \quad (1)$$

$$t_{DA} = \frac{0.0002637kt}{\phi\mu c_t A} \quad (2)$$

$$\frac{1}{q_D} = \frac{kh\Delta P}{141.2\mu B}\frac{1}{q} \quad (3)$$

$$\left[t_D * (1/q_D)'\right] = \frac{kh\Delta P}{141.2\mu B}\left[t * (1/q)'\right] \quad (4)$$

$$t_{DL} = \frac{t_D}{W_D^2} \quad (5)$$

$$W_D = \frac{Y_E}{r_w} \quad (6)$$

$$X_D = \frac{2b_x}{X_E} \quad (7)$$

$$Y_D = \frac{2b_y}{Y_E} \quad (8)$$

2.1 Characteristics lines and points for homogeneous reservoirs

2.1.1 Linear-flow regime

When the extreme reservoir boundaries are closed to flow and the well is off-centered inside the reservoir, the dominant flow regime is called linear (or single-linear) which is identified by a half slope on the curve of the derivative of the reciprocal rate. In Figure-2, a transition between linear and dual-linear flow regimes is observed since production tests take more time than pressure tests. The governing equation for this behavior is:

$$\frac{1}{q_D} = \frac{4\pi\sqrt{t_D}}{W_D} + s_L \quad (9)$$

Where s_L is the geometrical skin factor caused by the transition from dual-linear to linear flow regime. The derivative of Eq. 9 is:

$$\left[t_D * (1/q_D)'\right] = \frac{2\pi\sqrt{t_D}}{W_D} \tag{10}$$

Replacing Eqs. 1, 5 and 6 into Eq. 10 and solving for the k0.5YE product, it yields:

$$Y_E\sqrt{k} = \frac{14.4068B}{h\Delta P\left[t * (1/q)'\right]_L}\sqrt{\frac{\Delta t\mu}{\phi\, c_t}} \tag{11}$$

For Δt = 1 hr

$$Y_E\sqrt{k} = \frac{14.4068B}{h\Delta P\left[t * (1/q)'\right]_L}\sqrt{\frac{\mu}{\phi\, c_t}} \tag{12}$$

The skin factor caused by the convergence from linear to dual-linear flow regime is obtained by dividing Eq. 9 by 10. After plugging the dimensionless quantities and solving for sL:

$$s_L = \left(\frac{1/q}{\left[t * (1/q)'\right]_L} - 2\right)\frac{1}{9.8008 Y_E}\sqrt{\frac{k\, t_L}{\phi\, \mu\, c_t}} \tag{13}$$

Where $t_{L\ \text{is}}$ any convenient during the linear flow regime and $(1/q)_L$ and $[t*(1/q)']_L$ are the reciprocal rate and its derivative corresponding to t_L.

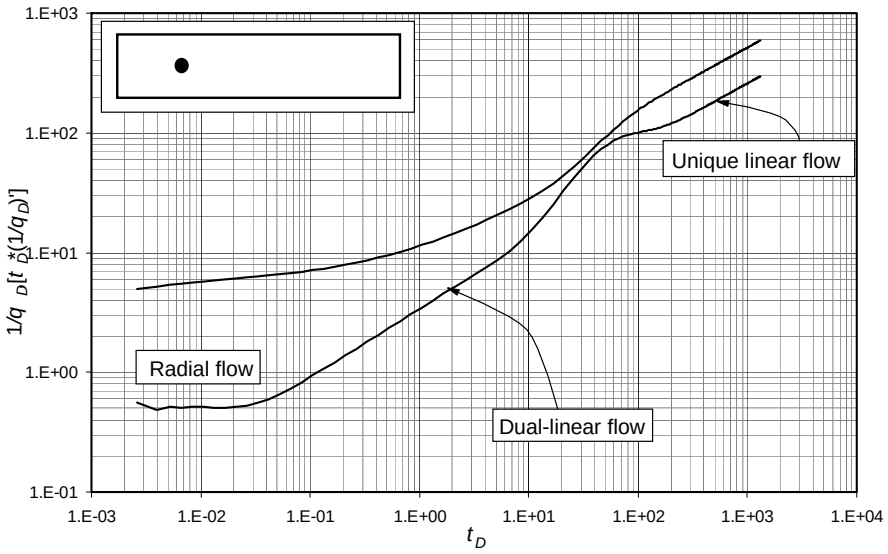

Figure-2. Linear flow regime for a well off-centered inside a closed boundary rectangular reservoir.

2.1.2 Dual-linear flow regime

This flow regime is presented for all the cases of closed, mixed and constant-pressure boundaries. It takes place when the well is located at any appropriate distance from the lateral boundaries. This behavior is shown in Figure-3. The governing dimensionless reciprocal rate and dimensionless derivative is, respectively,

$$\frac{1}{q_D} = \frac{5}{2}\frac{\sqrt{\pi t_D}}{W_D} + s_{DL} \tag{14}$$

$$\left[t_D * (1/q_D)'\right] = \frac{5}{4}\frac{\sqrt{\pi t_D}}{W_D} \tag{15}$$

Once the dimensionless quantities are replaced into Eq. 15, it yields:

$$Y_E\sqrt{k} = \frac{5.0801B}{h\Delta P\left[t * (1/q)'\right]_{DL}}\sqrt{\frac{\Delta t\mu}{\phi\, c_t}} \tag{16}$$

For Δt = 1 hr

$$Y_E\sqrt{k} = \frac{5.0801B}{h\Delta P\left[t * (1/q)'\right]_{DL}}\sqrt{\frac{\mu}{\phi\, c_t}} \tag{17}$$

As for the case of linear flow regime, the geometrical skin factor is obtained by dividing the reciprocal rate equation by the derivative equation:

$$s_{DL} = \left(\frac{1/q}{\left[t * (1/q)'\right]_{DL}} - 2\right)\frac{1}{27.7945 Y_E}\sqrt{\frac{k\, t_{DL}}{\phi\, \mu\, c_t}} \tag{18}$$

Where $t_{DL\ \text{is}}$ any convenient during the dual-linear flow regime and $(1/q)_{DL}$ and $[t*(1/q)']_{DL}$ are the reciprocal rate and its derivative corresponding to t_{DL}.

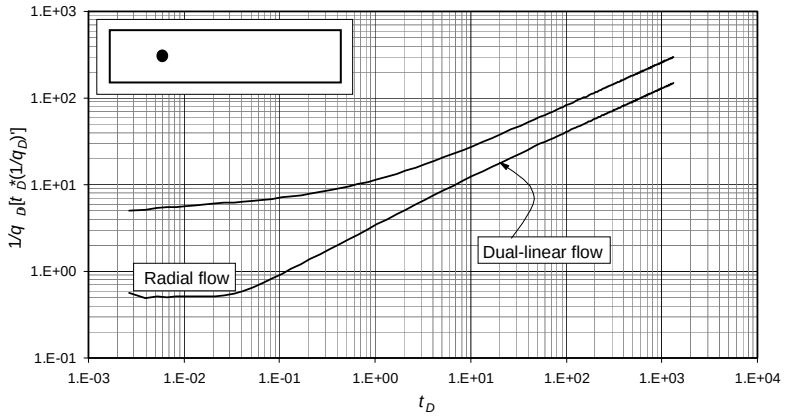

Figure-3. Dual-linear flow regime.

2.1.3 Parabolic flow

This flow regime is depicted in Figure-4 as a result of the combination of a constant-pressure boundary, when it is felt, and the travel of the perturbation along the other lateral side of the reservoir. The governing dimensionless reciprocal rate and reciprocal rate derivative are:

$$\frac{1}{q_D} = -\frac{\sqrt{\pi}}{4} W_D\left(X_D^2\right)\left(\frac{X_E}{Y_E}\right)^2 t_D^{-0.5} + s_{PB} \tag{19}$$

$$\left[t_D * (1/q_D)'\right] = \frac{\sqrt{\pi}}{8} W_D\left(X_D^2\right)\left(\frac{X_E}{Y_E}\right)^2 t_D^{-0.5} \tag{20}$$

After the dimensionless parameters are plugged in the former expression, we obtain:

$$\frac{k^{1.5} Y_E}{b_x^2} = 7705.9213\left(\frac{\mu B}{h\left[t * (1/q)'\right]_{PB}}\right)\left(\frac{\phi\,\mu\,c_t}{t_{PB}}\right)^{0.5} \tag{21}$$

The geometrical parabolic skin factor is obtained by dividing the reciprocal rate equation, Eq. 19, by the reciprocal rate derivative equation, Eq. 20:

$$s_{PB} = \left(\frac{1/q}{\left[t * (1/q)'\right]_{PB}} + 2\right)\frac{54.5745\, b_x}{Y_E}\sqrt{\frac{\phi\,\mu\,c_t}{k\,t_{PB}}} \tag{22}$$

Where t_{PB} is any convenient during the parabolic flow regime and (1/q) PB and [t*(1/q)'] PB are the reciprocal rate and its derivative corresponding to t_{PB}.

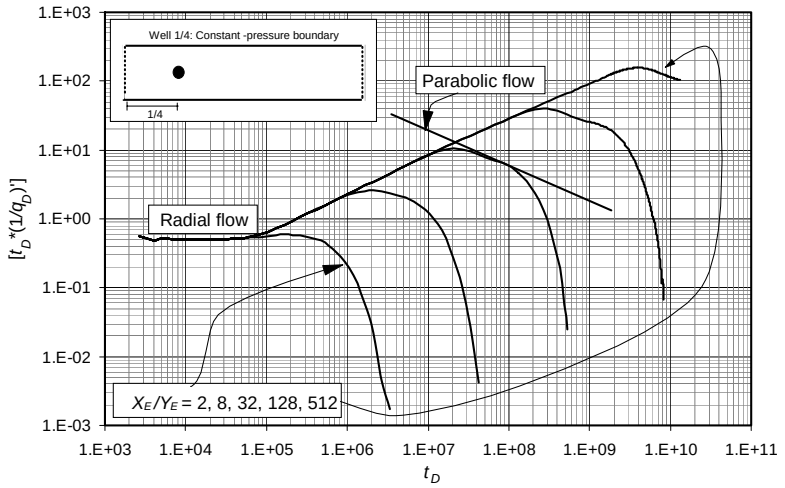

Figure-4. Parabolic flow regime.

2.1.4 Intersection points

2.1.4.1 Intersection between the pseudosteady-state line with the dual-linear, linear and radial lines

A unit-slope line is observed on the derivative during late times as shown in Figure-5. This line has the following governing equation:

$$\left[t_D * (1/q_D)'\right] = \frac{11}{2}\pi\, t_{DA} \tag{25}$$

The intercept of this line with the dual-linear, linear and radial lines allows, respectively, estimating reservoir drainage area, such as:

$$A = \sqrt{\frac{kt_{DLPSSi} Y_E^2}{62.3221\, \phi\, \mu\, c_t}} \tag{26}$$

$$A = \sqrt{\frac{kt_{LPSSi} Y_E^2}{501.2252\, \phi\, \mu\, c_t}} \tag{27}$$

$$A = \frac{kt_{RPSSi}}{109.7355\, \phi \mu c_t} \tag{28}$$

When the radial flow is masked but the hemi-radial flow is seen, the intersection of this line with the pseudosteady-state line leads to obtain:

$$A = \frac{kt_{RPSSi}}{219.4710\, \phi\, \mu\, c_t} \tag{29}$$

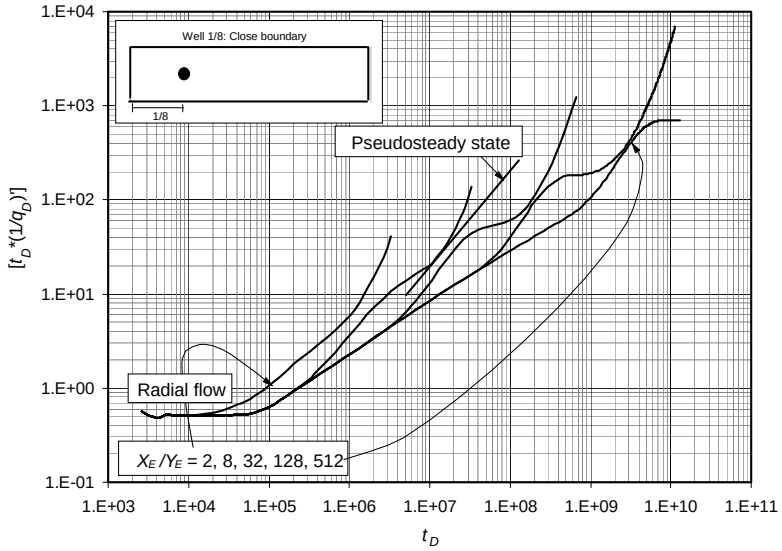

Figure-5. Reciprocal rate derivative showing the late-time pseudosteady-state period for a well at X_D = 1/8, inside a closed reservoir.

2.1.4.2 Intersection of the radial with dual-linear and linear lines

The intersection point between the infinite-acting reciprocal rate derivative and the dual-linear and linear lines allows obtaining expressions to estimate reservoir width. Therefore, if Eqs. 15 and 10 are equal to 0.5, Eq. 52; the following expressions are obtained once the dimensionless parameters are replaced:

$$Y_E = 0.07195\sqrt{\frac{kt_{RDLi}}{\phi\, \mu\, c_t}} \tag{30}$$

$$Y_E = 0.2040\sqrt{\frac{kt_{RLi}}{\phi\, \mu\, c_t}} \tag{31}$$

2.1.4.3 Intersection of the parabolic line with dual linear and linear lines

These intersection points are sketched in Figure-6, and they can be used to estimate the distance from the well to the closer lateral boundary, b_x.

$$b_x = \frac{1}{38.9470}\sqrt{\left(\frac{kt_{DLPBi}}{\phi\, \mu\, c_t}\right)} \tag{32}$$

$$b_x = \sqrt{\frac{Y_E}{109.2242}\left(\frac{kt_{RPB_i}}{\phi \mu c_t}\right)^{0.5}} \tag{33}$$

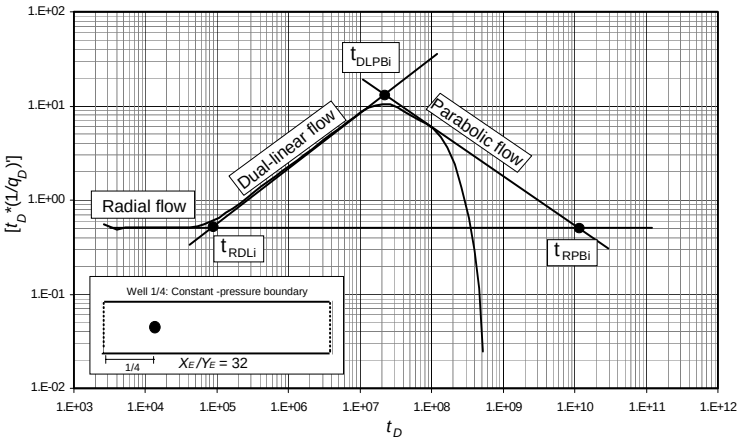

Figure-6. Derivative plot showing the parabolic flow and three intersection points.

2.1.4.4 Intersection of the negative-unit slope for mixed and constant-pressure boundaries when the well is near a constant-pressure boundary (dual linear, radial and parabolic)

When both lateral boundaries are subjected to constant-pressure once the dual-linear flow vanishes, the governing equation for the negative-unit slope, Figure-7, is governed by:

$$\left[t_D * (1/q_D)'\right] = \frac{4}{7\pi^2} W_D^2 \left(X_D^{1.5}\left(\frac{X_E}{Y_E}\right)^3 t_D^{-1}\right) \quad (34)$$

For the mixed-boundary case when the well is near the constant-pressure boundary, once the parabolic flow vanishes the derivative presents a hump before falling down. This also has a negative-unit slope which governing equation is:

$$\left[t_D * (1/q_D)'\right] = \frac{W_D^2}{\pi}\left(X_D^{1.5}\left(\frac{X_E}{Y_E}\right)^3 t_D^{-1}\right) \quad (35)$$

The intersection of the negative-unit slope lines, Eqs. 34 and 35, with the dual-linear, parabolic and radial lines leads to find the following expressions:

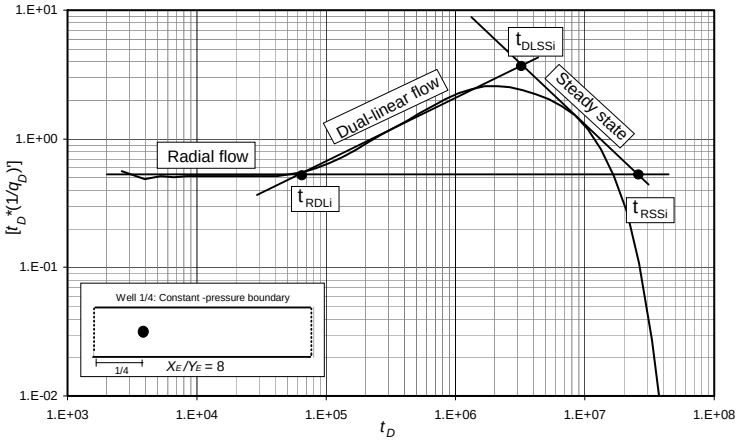

Figure-7. Derivative plot showing the steady-state period flow and three intersection points.

Constant-pressure boundaries

$$X_E^3 = \frac{1}{1.33\times10^9}\left(\frac{kt_{DLSSi}}{\phi\mu c_t}\right)^3 \frac{1}{b_x^3} \quad (36)$$

$$X_E^3 = \frac{1}{1.74\times10^6}\left(\frac{kt_{RSSi}}{\phi\mu c_t}\right)^2 \frac{Y_E^2}{b_x^3} \quad (37)$$

$$X_E^3 = \frac{1}{129.48}\left(\frac{kt_{PBSSi}}{\phi\ \mu\ c_t}\right) b_x \quad (38)$$

Mixed boundaries (well near the constant-pressure boundary)

$$X_E^3 = \frac{1}{9.02*10^9}\left(\frac{kt_{DLSSi}}{\phi\ \mu\ c_t}\right)^3 \frac{1}{b_x^3} \quad (39)$$

$$X_E^3 = \frac{1}{4.66*10^7}\left(\frac{kt_{RSSi}}{\phi\ \mu\ c_t}\right)^2 \frac{Y_E^2}{b_x^3} \quad (40)$$

$$X_E^3 = \frac{1}{3913.6439}\left(\frac{kt_{PBSSi}}{\phi\ \mu\ c_t}\right) b_x \quad (41)$$

2.1.5 Maximum points

Figure-8 shows the maximum points developed when the well is off-centered and near constant-pressure boundaries.

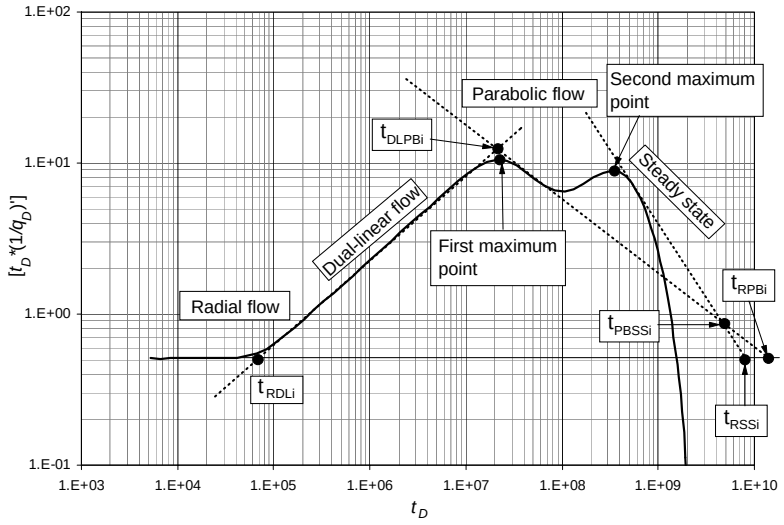

Figure-8. Derivative plot showing the parabolic flow, steady-state period flow, maximum points and intersection points.

These maximum points permit to determine reservoir area, A, reservoir length, X_E, and well location, b_x. The governing equations are:

First maximum point (Change from dual-linear to parabolic)

$$\left[t_D*(1/q_D)'\right]_{x1} = \frac{5}{4}\frac{\sqrt{\pi}}{W_D} t_{Dx1}^{0.5} \quad (42)$$

$$\frac{X_E}{Y_E} = \frac{5}{4}\left[\frac{\sqrt{\pi}}{W_D X_D}\right] t_{Dx1}^{0.5} \quad (43)$$

$$\frac{X_E}{Y_E} = \left[\frac{\sqrt{\pi}}{X_D}\right]\left[t_D*(1/q_D)'\right]_{x1} \quad (44)$$

Second maximum point (End of parabolic and start of steady-state)

$$\left[t_D*(1/q_D)'\right]_{x2} = \frac{\sqrt{\pi}}{W_D}\left(X_D^2\right) t_{Dx2}^{0.5} \quad (45)$$

$$\frac{X_E}{Y_E} = \left[\frac{\pi}{2X_D}\right] t_{Dx2}^{0.5} \quad (46)$$

$$\frac{X_E}{Y_E} = \left[\frac{\sqrt{\pi}}{2X_D^2}\right]\left[t_D*(1/q_D)'\right]_{x2} \quad (47)$$

After replacing the dimensionless parameters given by Eqs. 1, 5 and 6 into Eqs. 43 and 44, two equations for well position are obtained:

$$b_x = \left(\frac{1}{55.58}\right)\sqrt{\left(\frac{kt_{x1}}{\phi\mu c_t}\right)} \quad (48)$$

$$b_x = \frac{khY_E\Delta P\left[t*(1/q)'\right]_{x1}}{159.327\mu B} \quad (49)$$

Replacing the dimensionless parameters given by Eqs. 6 and 7 into Eqs. 48 and 49, two new equations are obtained for reservoir length estimation:

$$X_E = 637.3\left(\frac{b_x^2}{Y_E}\right)\left(\frac{\mu B}{\Delta P kh}\right)\left(\frac{1}{\left[t*(1/q)'\right]_{x2}}\right) \quad (50)$$

$$X_E = \frac{1}{39.2}\left(\frac{kt_{x2}}{\phi\ \mu\ c_t}\right)^{0.5} \quad (51)$$

Finally, during radial flow the reciprocal rate derivative is defined by:

$$\left[t_D*(1/q_D)'\right]=0.5 \quad (52)$$

Replacing Eq. 4 into Eq. 52 will result:

$$k=\frac{70.6\mu B}{h\Delta P\left[t*(1/q)'\right]} \quad (53)$$

where $(t*1/q')_r$ is the reciprocal rate derivative at any convenient time, t_r, during radial flow. The mechanical skin factor is obtained by dividing the reciprocal rate equation during radial flow assuming its behavior is the same as the pressure equation presented by Tiab (1993), therefore:

$$s_r=0.5\left(\frac{(1/q_r)}{\left[t*(1/q)'\right]_r}-\ln\left(\frac{kt_r}{\phi\mu c_t Y_E{}^2}\right)+7.43\right) \quad (54.a)$$

For a heterogeneous reservoir:

$$s_r=0.5\left(\frac{(1/q_r)}{\left[t*(1/q)'\right]_r}-\ln\left(\frac{kt_r}{\phi\mu c_t Y_E{}^2}\frac{1}{\omega}\right)+7.43\right) \quad (54.b)$$

2.2 Characteristics lines and points for heterogeneous reservoirs

2.2.1 Dual-linear flow regime

The found governing dimensionless reciprocal rate and reciprocal rate derivative equations for this flow regime are given by:

$$1/q_D=\frac{9}{4}\frac{\sqrt{\pi t_D}}{\sqrt{\omega}W_D}+s_{DL} \quad (55)$$

$$\left[t_D*(1/q_D)'\right]=\frac{9}{8}\frac{\sqrt{\pi\, t_D}}{W_D\sqrt{\omega}} \quad (56)$$

where s_{DL} ig Eq. 55 is the geometrical skin factor due to the convergence from radial to dual-linear flow. Substituting Eqs. 1, 4, and 6 into Eq. 56 and solving for the reservoir width;

$$Y_E=\frac{4.162115B}{h\Delta P\left[t*(1/q)'\right]_L}\sqrt{\frac{\mu\Delta t_{DL}}{k\phi c_t\omega}} \quad (57)$$

For Δt = 1 hr

$$Y_E=\frac{4.162115B}{h\Delta P\left[t*(1/q)'\right]_{DL}}\sqrt{\frac{\mu}{k\phi c_t\omega}} \quad (58)$$

As for the homogeneous case, the equation for the geometrical skin factor is:

$$s_{DL}=\left(\frac{(1/q)}{\left[t*(1/q)'\right]_{DL}}-2\right)\frac{1}{54.738732\,Y_E}\sqrt{\frac{kt_{DL}}{\phi\mu c_t\omega}} \quad (59)$$

2.2.2 Maximum and minimum points

Figure-9 presents the dimensionless rate derivative behavior against the dimensionless time for several values of λ and ω. Notice in that plot the existence of a characteristic maximum point once the dual-linear flow regime is interrupted by the transition period caused from heterogeneous to homogeneous behavior.

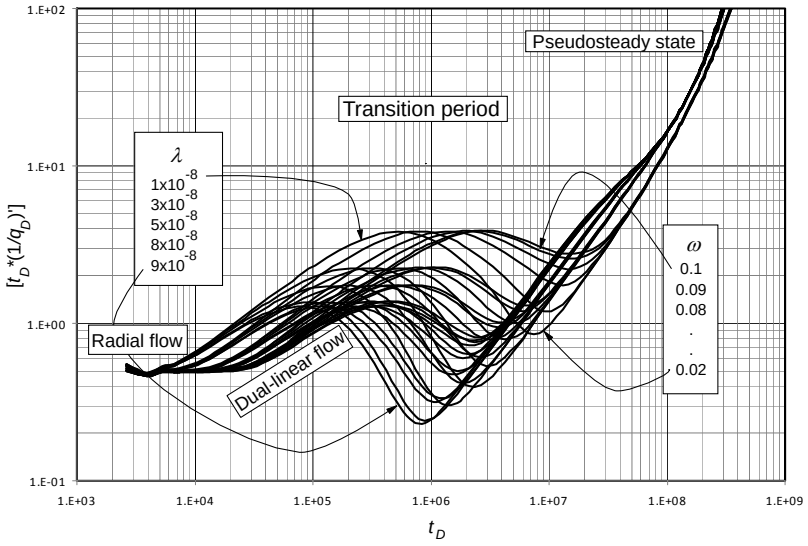

Figure-9. Dimensionless reciprocal rate derivative behavior vs. time for $1x10^{-8} \le \lambda \le 9x10^{-8}$ and $0.01 \le \omega \le 0.1$.

A unique maximum value of the reciprocal rate derivative is obtained when this is multiplied by the square root of the interporosity flow parameter as shown in Figure-10. The governing equation for this maximum point is:

$$\left[t_D*(1/q_D)'\right]_{\max}\lambda^{1/2}=0.0003876 \quad (60)$$

Replacing Eq. 4 into Eq. 60 and solving for the interporosity flow parameter,

$$\lambda=\left[\frac{0.05472912\mu B}{kh\Delta P\left[t*(1/q)'\right]_{\max}}\right]^2 \quad (61)$$

In order to derive a correlation of ω as a function of $1/q_D$, (t_D*$1/q_D$') and t_D for a given value of λ a plot of the dimensionless reciprocal rate and its derivative against time was built, see Figure-12, and different derivative minimum values were read from that plot to give the following relationship which has a correlation coefficient of 0.9998:

$$\omega=\frac{a+b\ln\left(t_D*1/q_D'\right)_{\min}+c\left(\ln\left(t_D*1/q_D'\right)_{\min}\right)^2+d\left(\ln\left(t_D*1/q_D'\right)_{\min}\right)^3+e\ln\lambda}{1+f\ln\left(t_D*1/q_D'\right)_{\min}+g\left(\ln\left(t_D*1/q_D'\right)_{\min}\right)^2+h\left(\ln\left(t_D*1/q_D'\right)_{\min}\right)^3+i\ln\lambda} \quad (62)$$

Where;

a = -0.15407418	b = -0.0039050889	c = 0.0022251207
d = 4.2193304x10^{-4}	e = -0.0079273861	f = 0.2804578
g = -0.072289158	h = 0.023141728	i = 0.07200547

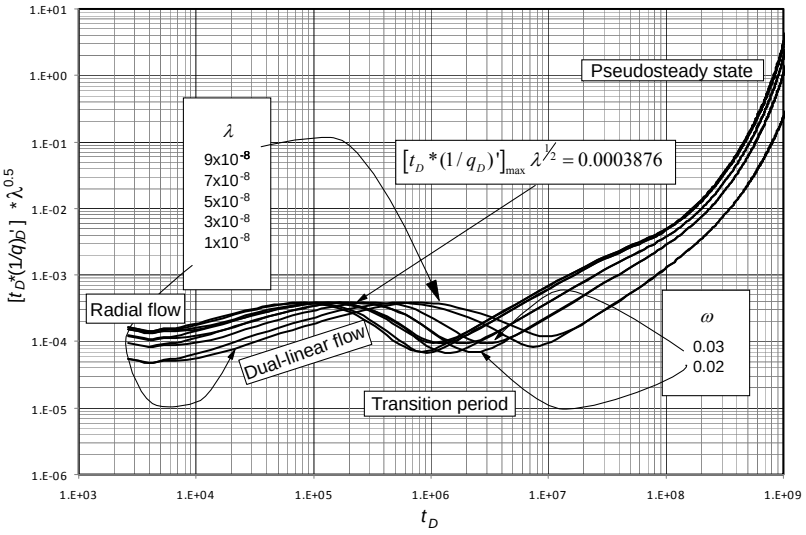

Figure-10. Effect of the square root of λ on the maximum point of the reciprocal rate derivative.

2.2.3 Intersection point between the pseudo steady-state and dual-linear lines

Equating Eq. 25 with 56, then, plugging the dimensionless quantities and solving for reservoir drainage area, it yields:

$$A=0.140998\sqrt{\frac{Y_E^2\omega k t_{DLPSSi}}{\phi\mu c_t}} \quad (63)$$

Being t_{DLPSSi} the intersection time between the dual-linear flow regime and the pseudosteady-state period lines.

2.2.4 Intersection point between the radial and dual-linear lines

According to Eq. 52, the infinite-acting radial line has a dimensionless value of 0.5 during radial flow regime. If this value is set equal to the reciprocal rate derivative of the dual-linear equation extrapolated to the radial flow value, it allows to obtain an expression to find reservoir width once the dimensionless parameters have been replaced,

$$Y_E=0.0648256\sqrt{\frac{k\,t_{RDLi}}{\phi\mu c_t\omega}} \quad (64)$$

Being t_{RDLi} the intersection time between the radial and dual-linear flow regime lines,

2.2.5 Intersection point between the radial and Pseudosteady-state lines

Again, Eq. 28 is obtained from manipulation of Eq. 52 and 25.

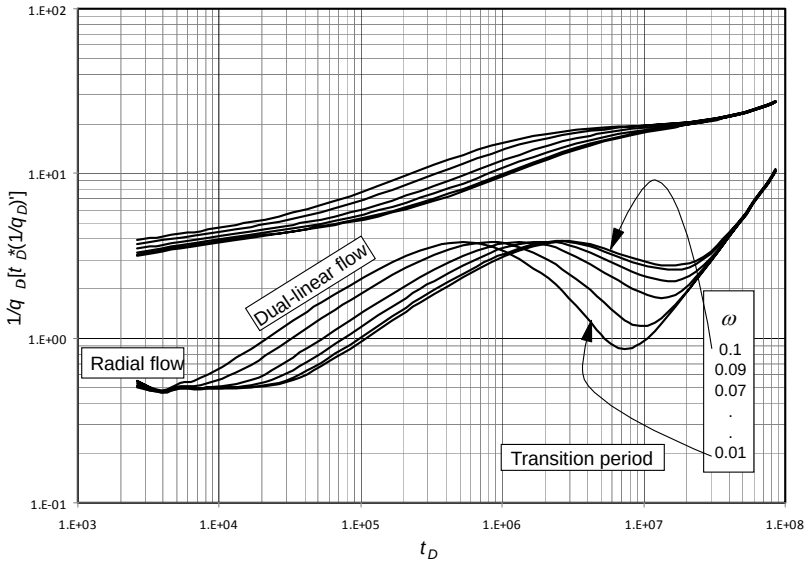

Figure-11. Effect of ω on the minimum point of the reciprocal rate derivative for $\lambda = 1x10^{-8}$.

2.2.6 Linear flow regime occurs after the transition period

When the linear flow occurs after the transition period, the linear behavior corresponds to a homogeneous reservoir as depicted in Figure-12. For this case the governing equation is Eq. 9, therefore, expressions derived from Eq. 9 also corresponds to this analysis.

2.2.7 Linear flow regime occurs before the transition period

As shown in Figure-13, the linear flow regime is still affected by the heterogeneous behavior, then, the reciprocal rate and its derivative are defined here as:

$$\frac{1}{q_D} = \frac{21}{5}\frac{\sqrt{\pi\, t_D}}{W_D\sqrt{\omega}} + s_L \tag{65}$$

$$\left[t_D*(1/q_D)'\right] = \frac{21}{10}\frac{\sqrt{\pi\, t_D}}{W_D\sqrt{\omega}} \tag{66}$$

As stated before, Eqs. 64 and 65 allow obtaining:

$$Y_E = \frac{42.480763\, B}{h\Delta P\left[t*(1/q)'\right]_L}\sqrt{\frac{\mu\, t_{DL}}{k\phi\, c_t\omega}} \tag{67}$$

$$s_L = \left(\frac{1/q}{\left[t*(1/q)'\right]_L} - 2\right)\frac{1}{29.32416\, Y_E}\sqrt{\frac{k\, t_{DL}}{\phi\mu c_t\omega}} \tag{68}$$

As described by Figure-14, there exists a direct relationship between the square root of the interporosity flow parameter multiplied by the reciprocal rate derivative against the maximum point. This allows obtaining the following expression:

$$\sqrt{\lambda}\left[t_D*(1/q_D)'\right]_{\max} = 0.000746 \tag{68}$$

Solving for λ from Eq. 68 once the respective dimensionless group is replaced, it yields:

$$\lambda = \left[\frac{0.105335\mu B}{kh\Delta P\left[t*(1/q)'\right]_{\max}}\right]^2 \tag{69}$$

From Figure-15, readings of the minimum point for different values of the interporosity flow parameter and the dimensionless storativity coefficient were correlated to obtain an expression which has a correlation coefficient of 0.99987.

$$\omega = \frac{a + b\ln\lambda + c\ln\lambda^2 + d\left(t_D*1/q_D'\right)_{\min} + e\left(t_D*1/q_D'\right)^2_{\min} + f\left(t_D*1/q_D'\right)^3_{\min}}{1 + g\ln\lambda + h\left(t_D*1/q_D'\right)_{\min} + i\left(t_D*1/q_D'\right)^2_{\min} + j\left(t_D*1/q_D'\right)^3_{\min}} \tag{70}$$

a = 0.14646803 b = 0.013342717 c = 0.00030434555
d = -0.00026701191 e = 2.4497641x10^{-6} f = -9.2559594x10^{-9}
g = 0.049793248 h = 0.0021617165 i = -8.3473003x10^{-6}
j = 8.9505062x10^{-9}

Finally, the unit-slope line during the transition period was correlated (r^2 = 0.9923) to obey the following governing equation:

$$\lambda = a + b\ln t_{D,usi} + d(\ln t_{D,us})^2 + f\ln t_{D,usi} + g(\ln t_{D,usi})^3 + i\ln t_{D,usi} + j(\ln t_{D,usi})^2 \ln y \quad (71)$$

a= 0.0000172772864496202 b= -3.671446810044302x10^{-06}
d= 2.27459107228314x10^{-07} f= 3.53205100139827x10^{-07}
g= -4.737297387478569x10^{-09} i= -9.98959453867718x10^{-09}
j= -1.13570599631755x10^{-08}

where *usi* is the intercept of the unit-slope line during the transition period with the radial flow line. λ may also be estimated by the equation introduced by Tiab and Escobar (2003):

$$\lambda = \frac{3792(\phi c_t)_t \mu r_w^2}{k\Delta t_{\min}}\left[\omega \ln\left(\frac{1}{\omega}\right)\right] \quad (72)$$

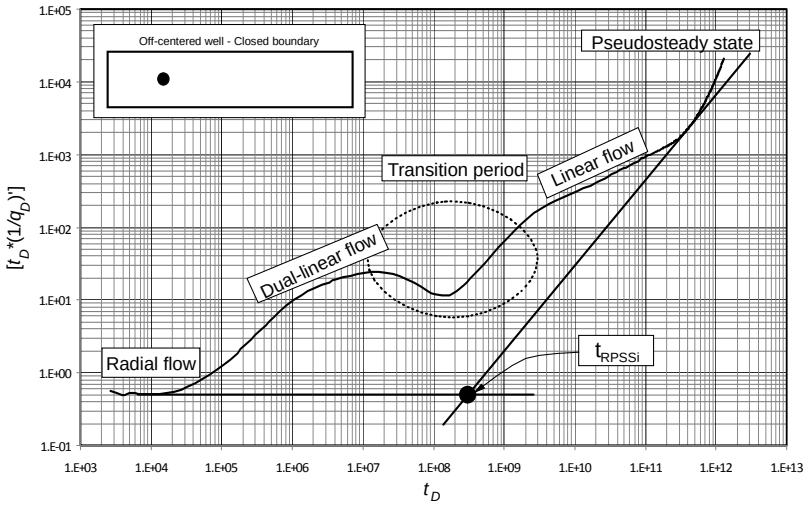

Figure-12. Linear flow regime after the transition period.

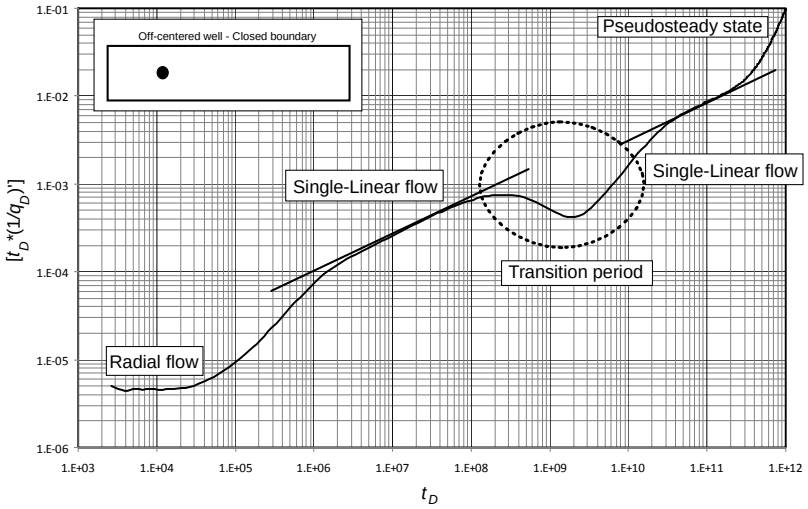

Figure-13. Linear flow regime before the transition period.

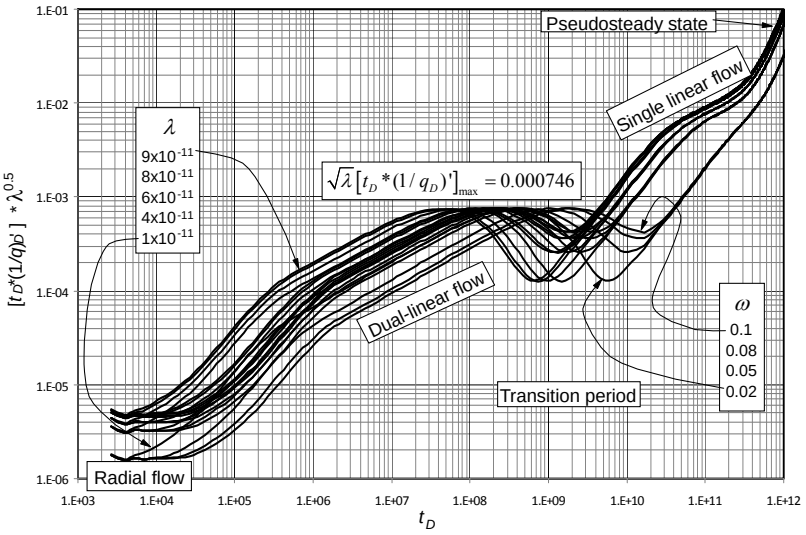

Figure-14. Relationship between the square root of the interporosity flow parameter times the reciprocal rate derivative and the maximum point.

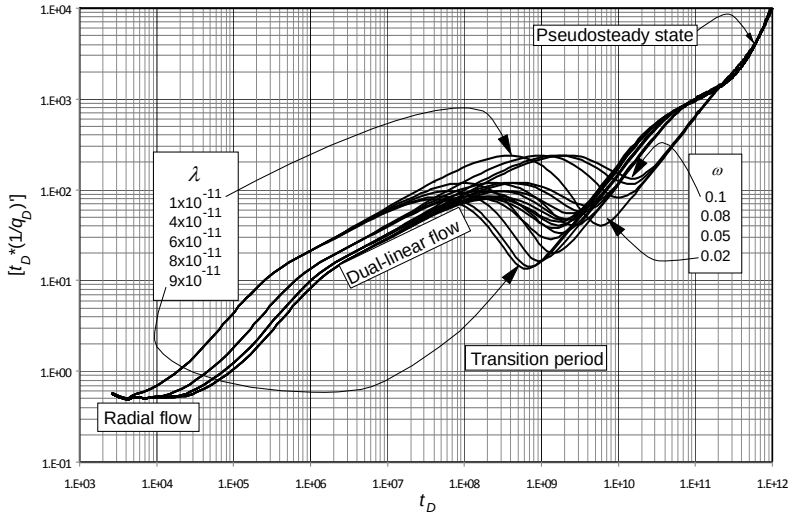

Figure-15. Effect of ω and λ on the minimum point.

3. EXAMPLES

Examples 1 to 5 were simulated with the input data of Table-1. The results along with the used equations are given in Table-2.

3.1 Synthetic example 1 - homogeneous reservoir

Both lateral boundaries are subjected to constant pressure and the well is off-centered. Reciprocal rate and reciprocal rate derivative are given in Figure-16. From this plot, the following information was read:

$(t*1/q')_r$ = 6.94x10-6 D/STB	t_{DL} = 5.0357 hr	$(t*1/q')_{DL}$ = 2.43x10-5 D/STB
t_{RDLi} = 0.5035 hr	t_{DLPBSi} = 16 hr	t_{RPBSi} = 600 hr
t_{DLSSNi} = 25 hr	t_{RSSNi} = 165 hr	

The estimated parameters along with the number of the used equation are reported in Table-2.

3.2 Synthetic example 2 - homogeneous reservoir

In this case, both lateral boundaries are closed to flow and the well is off-centered. Then, pseudosteady-state is developed. The reciprocal rate and reciprocal rate derivative are given in Figure-17 from which the below data was obtained:

$(t*1/q')_i$ = 6.93*10-6 D/STB	t_{DL} = 10.04 hr	t_{DLPSSi} = 165 hr
$(t*1/q')_{DL}$ = 3.62*10-5 D/STB	t_L = 400 hr	t_{LPSSi} = 1500 hr
$(t*1/q')_L$ = 7.04x10-4 D/STB	t_{RPSSi} = 7.5 hr	t_{RDLi} = 0.4 hr
t_{RLi} = 0.035 hr		

As for the former example, the results of estimated parameters along with the number of used equation are reported in Table-2.

Table-1. Input data for the examples.

Parameter	Synthetic example					Field example
	1	2	3	4	5	
ΔP, psi	5000	5000	5000	2500	5000	2800
μ, cp	2					1.52
ϕ, %	20					13
B, rb/STB	1.2					1.04
c_t, psi^{-1}	$1x10^{-6}$					$4.34x10^{-5}$
r_w, ft	0.5					0.3
h, ft	100					
X_E, ft	4000	16000	16000	20000	680000	
Y_E, ft	500	500	500	1000	1000	
b_x, ft	1000		2000			
k, md	50					65
λ				$5x10^{-8}$	$4x10^{-11}$	$4x10^{-8}$
ω				0.02	0.1	0.21
s_r						-2.3

Table-2. Results for synthetic examples.

Para-meter	Synthetic example									
	1		2		3		4		5	
	Eq.	Value	Eq.	Value	Eq.	Value	Eq.	Value	Eq.	Value
k, md	53	49.83	53	48.9	48.97	53	53	52.14	53	48.8
Y_E, ft	31	564.1	11	482.6			58	979.2	67	1048.5
Y_E, ft	16	509.5	16	444.2	16	459.3				
Y_E, ft			30	503.1						
Y_E, ft			31	422						
b_x, ft	32	1148.3			48	1427.4				
b_x, ft	33	1119.7			49	2334				
X_E, ft	36	4678.6			36	15102.4				
X_E, ft	37	3939.1			37	14467.5				
X_E, ft					50	15737.9				
s_r	54.a	0.19	54.a	0.18	54.a	1.35	54.b	-2.2		
s_{DL}	18	4.93	18	4.54	18	4.07	59	6.74		
s_L			13	-23.5						
s_{PB}	21	0.0133			21	0.013				
A, ft^2			26	206.5			63	402.8	28	10251.6
A, ft^2			27	219.6						
A, ft^2			28	191.8						
ω							62	0.0214	62	0.0996
λ							61	$4.64x10^{-8}$	61	$4.14x10^{-11}$

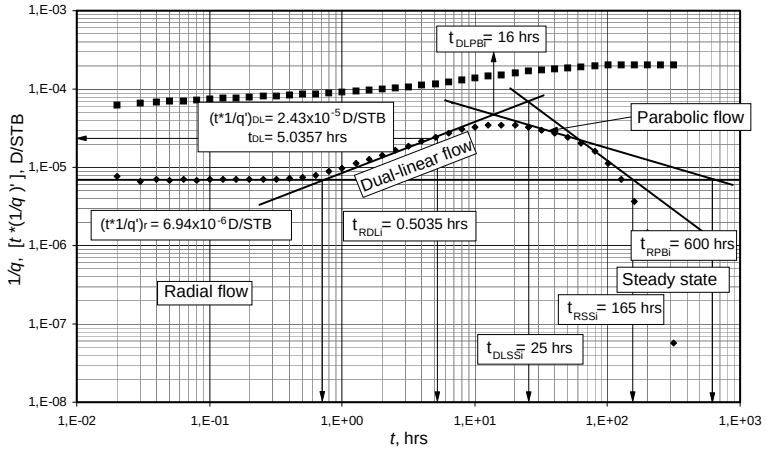

Figure-16. Reciprocal rate and reciprocal rate derivative for synthetic example 1.

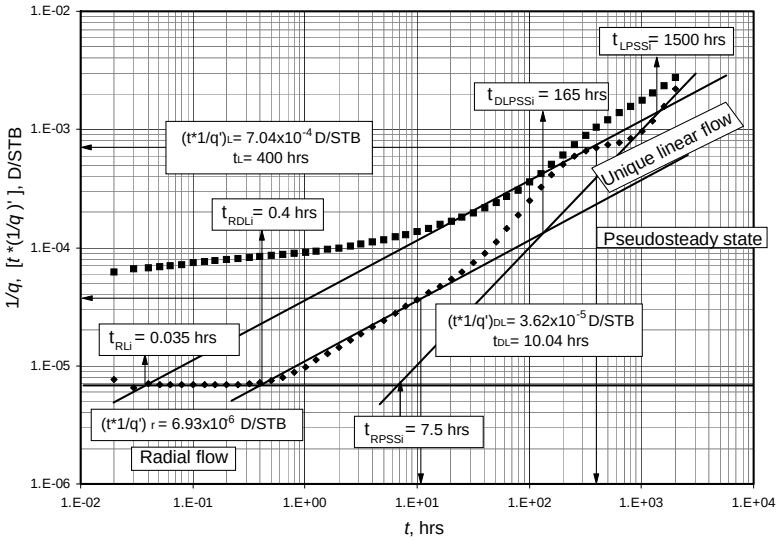

Figure-17. Reciprocal rate and reciprocal rate derivative for synthetic example 2.

3.3 Synthetic example 3 - homogeneous reservoir

Figure-18 presents the data of reciprocal rate and its derivative for a well near a constant-pressure boundary and the other lateral boundary is closed to flow. From this plot the below information was obtained:

$(t*1/q')_r$ = 6.92x10-6	t_{DL} = 20.04 hr	$(t*1/q')_{DL}$ = 5.37x10-5
t_{RDLi} = 0.35 hr	$(t*1/q')_{X1}$ = 7.14x10-5	t_{X1} = 50.35 hr
t_{DLPBi} = 50.4 hr	t_{RPBi} = 6004.8 hr	t_{DLSS1i} = 503 hr
t_{RSS1i} = 17000 hr	$(t*1/q')_{X2}$ = 3.11x10-5	t_{X2} = 3004.74 hr

Again, the results for this example and the number of used equation are reported in Table-2.

3.4 Synthetic example 4-heterogeneous reservoir

In this case, both lateral boundaries are closed to flow. In this case the dual-linear flow regime is interrupted by the heterogeneity. Therefore, pseudosteady-state is expected to develop if the test is long enough. The reciprocal rate and reciprocal rate derivative are given in Figure-19 from which the below data was obtained:

$(t*1/q')_r$ = 1.30x10-5	t_{DL} = 0.2523 hr	$(t*1/q')_{DL}$ = 3.16x10-5
$(1/q')_r$ = 1.12x10-4	$(1/q')_{DL}$ = 1.55x10-5	t_{DLPSSi} = 6000 hr
t_r = 0.03 hr	$(t*1/q')_{max}$ = 4.68x10-5	t_{RDLi} = 0.035 hr
$(t*1/q')_{min}$ = 8.19x10-5		

The estimated parameters are also reported in Table-2 along with the number of the used equation.

3.5 Synthetic example 5 - heterogeneous reservoir

Figure-20 contains data of the reciprocal rate and the reciprocal rate derivative against time for an elongated naturally reservoir in which the linear flow regime was interrupted by the transition period. The following readings were obtained from Figure-20.

$(t*1/q')_r$ = 6.95x10-6	t_L = 200 hr	$(t*1/q')_L$ = 6.24x10-4
$(1/q')_r$ = 8.84x10-5	$(1/q')_L$ = 1.26x10-3	t_{RPSSi} = 402 hr
t_r = 0.07981 hr	(t*1/q')max = 1.61x10-3	tLPSSi = 2000000 hr
(t*1/q') min = 9.11x10-4		

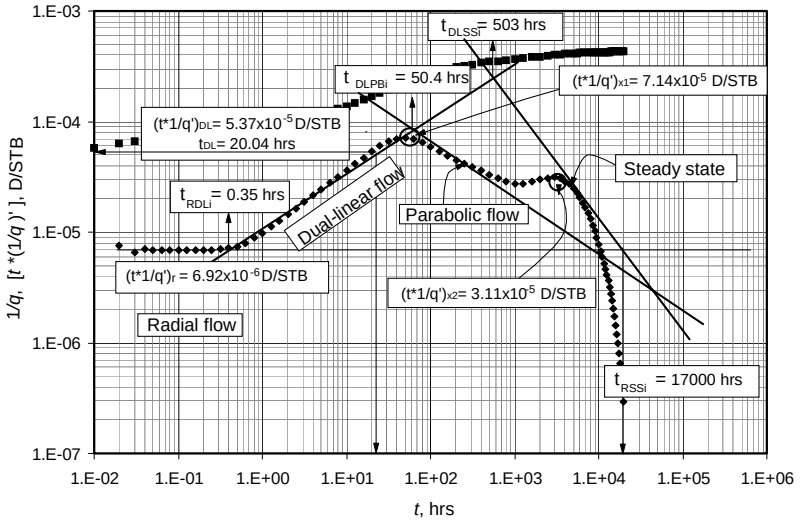

Figure-18. Reciprocal rate and reciprocal rate derivative for synthetic example 3.

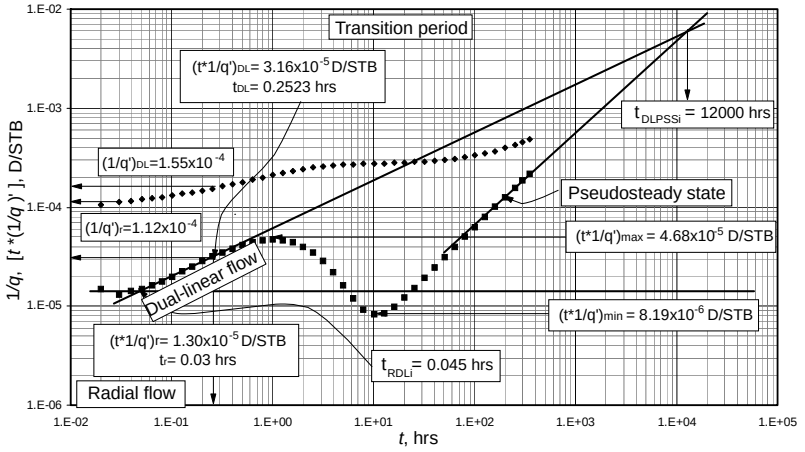

Figure-19. Reciprocal rate and reciprocal rate derivative for synthetic example 4.

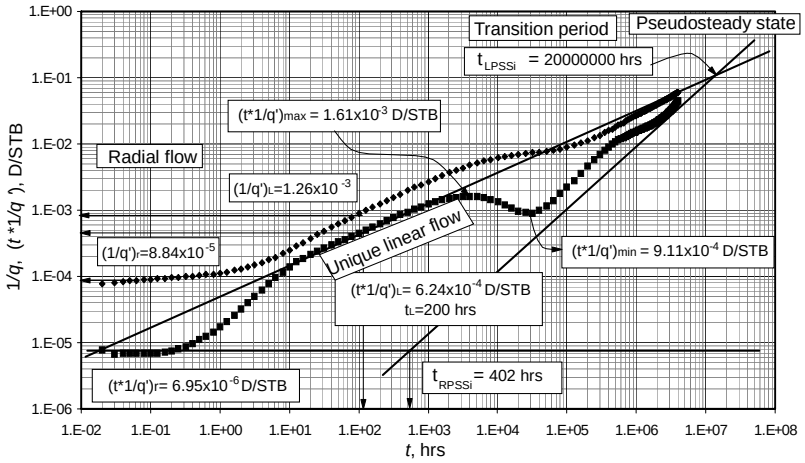

Figure-20. Reciprocal rate and reciprocal rate derivative for synthetic example 5.

3.6 Field example-heterogeneous reservoir

Marhaendrajana *et al*. (2004) presented a field case for a naturally fractured system which input information is given in Table-1 and reciprocal rate and its derivative vs. time is given in the Figure-21. The following data was obtained from Figure-21.

t_{RDLi} = 0.032 hr $(t^*1/q')_{DL}$ = 2x10^{-4} hr t_{DL} = 12.66 hr
t_{DLRi} = 0.0105 hr t_{min} = 39.3 hr

The first step, for this exercise is to estimate ω using Eq. 70. This value is then used used in Eqs. 57 and 64 to estimate reservoir width and the dual-linear skin factors, Eq. 59. Because of the noise in the data is not possible to obtain a clear value of the maximum point on the pressure derivative, then,λ is estimated using the minimum point with Eq. 72. It can be seen that the data is so noisy and the radial flow regime is unclear. Using the permeability, given in Table-1, the derivative during radial flow regime, $(t^*1/q')_r$, can be estimated from Eq. 52:

$$\left[t*(1/q)'\right]_r = \frac{70.6\mu B}{h\Delta Pk} = \frac{70.6(1.52)(1.04)}{(100)(2800)(65)} = 6.13\times10^{-6}\,\text{md}$$

With this value and the first $(1/q)$ value is possible to estimate the mechanical skin factor with Eq. 54.b. This problem was also solved by Escobar *et al*. (2010). All the values are reported in Table-3.

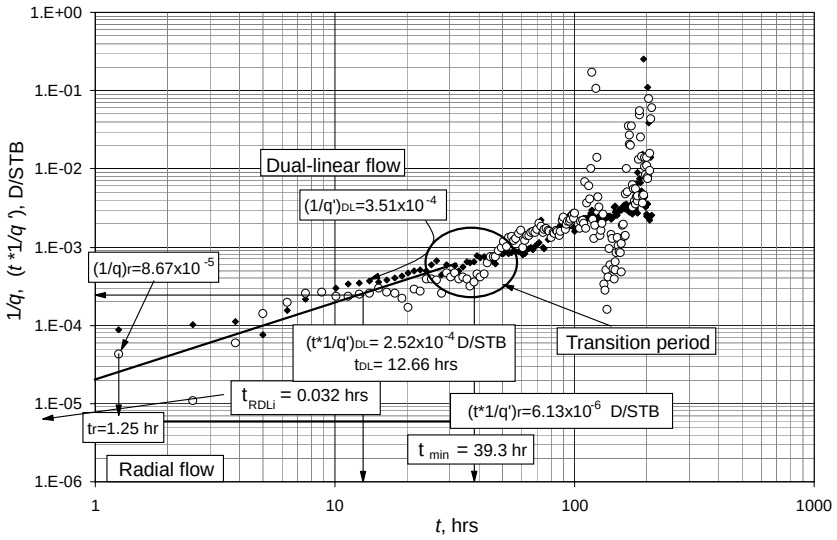

Figure-21. Reciprocal rate and reciprocal rate derivative for the field case.

Table-3. Results for field example.

Parameter	Escobar *et al.* (2010)	Marhaendrajana *et al.* (2004)	This work
λ	1.94x10^{-7}	4x10^{-8}	8.28x10^{-8}
ω	0.06	0.2	0.018
s_r	N.C.	-2.2	-0.46
s_{DL}	72	N.C.	-5.85
Y_E, ft	122.7	N.C.	138.4
Y_E, ft	N.C.	N.C.	133.03

4. ANALYSIS OF RESULTS

The simulated examples indicate that the proposed equations provide results which are in good agreement with the input data. For the actual field case of a heterogeneous reservoir, the reservoir width agrees closely with the results from Escobar *et al*. (2010). The interporosity flow parameters matches the values from the three sources, but the dimensionless storativity coefficient do not agree with the result from Marhaendrajana *et al*. (2004) but the difference is acceptable and are due to the noisy data.

Nomenclature

B	Oil formation factor, rb/STB
b	Intercept
b_x	Well position inside the reservoir
c_t	Total system compressibility, 1/psi
h	Formation thickness, ft
k	Permeability, md
m	Slope
P_i	Initial reservoir pressure, psi
P_{wf}	Well-flowing pressure, psi
P	Pressure, psi
s	Skin factor
s_r	Mechanical skin factor
t	Time, hr
W_D	Dimensionless reservoir width
X_D	Dimensionless well position along the *x*-axis
X_E	Reservoir length, ft
Y_D	Dimensionless well position along the *y*-axis
Y_E	Reservoir width, ft
$1/q$	Reciprocal flow rate, D/STB
$1/q_D$	Dimensionless reciprocal flow rate

Greek

ω	Dimensionless storativity coefficient, $(\phi c_t)_f/[(\phi c_t)_m+(\phi c_t)_f]$
Δ	Change, drop
ϕ	Porosity
λ	Interporosity flow parameter
ρ	Densidad, lbm/ft^3
μ	Oil viscosity, cp

Suffices

1, 1*r*, *er*	Primer régimen de flujo o temprano
D	Dimensionless
DL	Dual linear, dimensionless based on width
DLPBi	Dual linear and parabolic intercept
DLPSSi	Dual linear and pseudosteady-state intercept
DLSSi	Dual linear and steady-state intercept
L	Linear
*L*1	Lineal temprano a 1 hr
LPSSi	Linear and pseudosteady-state intercept
max	Maximum
min	Minimum
PB	Parabolic
PBSSi	Parabolic and steady-state intercept
RDLi	Radial and dual linear intercept
RLi	Radial and linear intercept
RPBi	Radial and parabolic intercept
RPSSi	Radial and pseudosteady-state intercept
RSSi	Radial and steady-state intercept
usi	Intercept of the radial line with the int-slope line during

	the transition period
$x1$	First maximum between dual-linear and parabolic flow regimes
$x2$	Second maximum between end of parabolic and start of steady-state
w	Well

5. CONCLUSIONS

The *TDS* methodology for rate transient analysis was complemented with new equations for long and narrow homogeneous and naturally fractured reservoirs. The equations were successfully applied to synthetic examples. A field example for a heterogeneous reservoir was presented to demonstrate the application of the proposed solution.

ACKNOWLEDGEMENTS

The authors would like to thank the Universidad Surcolombiana and Ecopetrol-ICP for providing support for the completion of this work. We strongly thank Dr. Taufan Marhaendrajana for providing the field example to us.

REFERENCES

El-Banbi A.H. and Wattenberger R.A. 1998. Analysis of Linear Flow in Gas Well Production. Paper SPE 39972 Gas Technology Symposium, Alberta, Canada, March 15-18.

Escobar F.H., Hernández Y.A. and Hernández C.M. 2007. Pressure Transient Analysis for Long Homogeneous Reservoirs using *TDS* Technique. Journal of Petroleum Science and Engineering. 58(1-2): 68-82.

Escobar F.H., Munoz O.F., Sepulveda J.A. and Montealegre M. 2005. New Finding on Pressure Response In Long, Narrow Reservoirs. CT and F - Ciencia, Tecnología y Futuro. 2(6).

Escobar F.H. and Montealegre-M. M. 2006. Effect of Well Stimulation on the Skin Factor in Elongated Reservoirs. CT and F - Ciencia, Tecnología y Futuro. 3(2): 109-119. Dec.

Escobar F.H. and Montealegre M. 2007. A Complementary Conventional Analysis For Channelized Reservoirs. CT and F - Ciencia, Tecnología y Futuro. 3(3): 137-146. Dec.

Escobar F.H. 2008. Petroleum Science Research Progress. Nova Publishers. Edited by Korin L. Montclaire. Recent Advances in Well Test Analysis for Long a Narrow Reservoirs.

Escobar F.H., Rojas M.M. and Cortés G.J. 2010. Straight-Line Conventional Transient Rate Analysis for Long Homogeneous and Heterogeneous Reservoirs. Article sent to DYNA Journal to request publication.

Raghavan R. And Chu W.C. 1966. On the Determination of Reservoir Pressure when Radial-Flow Conditions are Nonexistent. Paper SPE 35619, Gas Technology Conference held in Calgary, Alberta, Canada.

Marhaendrajana T., Blasingame T.A. and Rushing J.A. 2004. Use of Production Data Inversion to Evaluate Performance of Naturally Fractured Reservoirs. Paper SPE 90013, SPE International Petroleum Conference, Puebla, Mexico. 8-9 November.

Massonet G.J., Norris R.J. and Chalmette J-C. 1993. Well Test Interpretation in Geologically Complex Channelized Reservoirs. Paper SPE 26464, 68th Annual Technical Conference and Exhibition of the Society of Petroleum Engineers held in Houston, TX.

Nutakki R. and Mattar L. 1982. Pressure Transient Analysis of Wells in Very Long Narrow reservoirs. Paper SPE 11221, presented at the 57th Annual Fall Technical Conference and Exhibition of the Society of Petroleum Engineers held in Dallas, TX.

Tiab D. and Escobar F.H. 2003. Determinación del Parámetro de Flujo Interporoso a Partir de un Gráfico Semilogarítmico. X Congreso Colombiano del petróleo (Colombian Petroleum Symposium). October 14-17, Bogotá (Colombia).

TIAB D. 1993. Analysis of Pressure and Pressure Derivative without Type-Curve Matching: 1- Skin Factor and Wellbore Storage. Paper SPE 25423 presented at the Production Operations Symposium held in Oklahoma City, OK. March 21-23.

Warren J.E. and Root P.J. 1963. The Behavior of Naturally Fractured Reservoirs. Soc. Pet. Eng. J., September. pp. 245-255.